INTERNATIONAL JOURNAL FOR NUMERICAL AND ANALYTICAL METHODS IN GEOMECHANICS
Int. J. Numer. Anal. Meth. Geomech. 2011; **35**:569–585
Published online 20 April 2010 in Wiley Online Library (wileyonlinelibrary.com). DOI: 10.1002/nag.909

Numerical and analytical observations on long and infinite slopes

D. V. Griffiths, Jinsong Huang*, † and Giorgia F. deWolfe

Division of Engineering, Colorado School of Mines, Golden, CO, U.S.A.

SUMMARY

Interest in the mechanics of landslides has led to renewed evaluation of the infinite slope equations, and the need for a more general framework for estimating the factor of safety of long and infinite slopes involving non-homogeneous soil profiles. The paper describes finite element methods that demonstrate the potential for predicting failure in long slope profiles where the critical mechanism is not necessarily at the base of the soil layer. The influence of slope angle is also examined in long slopes, leading to some counter-intuitive conclusions about the impact of slope steepness on the factor of safety. Copyright © 2010 John Wiley & Sons, Ltd.

Received 15 October 2009; Revised 25 January 2010; Accepted 28 January 2010

KEY WORDS: infinite slope; stability; finite element method

1. INTRODUCTION

The paper reviews the familiar infinite slope stability equations and describes the development of powerful general-purpose finite element programs for computing the factor of safety of long and infinite slopes. The motivation for this development comes from a renewed interest in the mechanics of shallow landslides (e.g. [1]) and the need for a more general approach to the analysis of long slopes allowing soil properties and groundwater conditions to vary with depth. Conventional use of the infinite slope equations on soils involving both cohesion and friction gives a factor of safety that assumes a homogeneous soil profile and a critical failure plane running parallel to the ground surface at the full depth of the soil layer.

Some of the previous work on this subject has focused on shear mechanisms and states of stress in an infinite slope (e.g. [2]), as well as analysis of 1-D and 2-D strains and displacements (e.g. [3–5]). More specifically, a finite element approach to long slopes based on limit equilibrium theory and strain softening behavior has been presented by Runesson and Wiberg [6] and Wiberg [7]. Another group of investigators have studied the influence of groundwater flow and lateral (3-D) flow fields in relation to landslides (e.g. [8–10]) as well as estimating the influence, using an infinite slope analysis, of infiltration on surficial slope stability (e.g. [11–13]). More recently, Yang [14] considered the influence of horizontal acceleration on the seismic stability of landslides via the infinite slope equations.

For soils with variable soil strength and pore pressure profiles, the infinite slope equations cannot be used directly to find the factor of safety. Instead, an algorithm is needed that can examine all potential failure planes until a minimum factor of safety is found. In these cases, the critical failure plane may not occur at the bottom of the soil layer, but at some intermediate depth.

*Correspondence to: Jinsong Huang, Division of Engineering, Colorado School of Mines, Golden, CO, U.S.A.
†E-mail: jhuang@mines.edu

Contract/grant sponsor: NSF; contract/grant number: CMS-0408150

The elasto-plastic finite element method has been applied successfully by numerous investigators to conventional slope stability analysis using strength reduction (e.g. [15–18]), and shown to offer several advantages over conventional limit equilibrium techniques. In particular, the method is able to 'seek out' the critical failure surface without user intervention and display deformations. This paper seeks to exploit the same concepts in the analysis of long and infinite slopes.

2. REVIEW OF THE INFINITE SLOPE EQUATIONS

The infinite slope equations are described in detail in other publications (e.g. [19–22]); however, to set the scene for the numerical analyses to follow and for consistency of notation we present a brief review in this section.

The key assumption in an infinite slope analysis is that the slope is very long relative to the vertical depth (H) of the potential failure surface. When considering force equilibrium of a typical slice within a long slope as shown in Figure 1, the side forces on each side of the slice can be considered equal and opposite, hence their magnitude does not need to be known since they cancel out. Any vertical column of soil within the infinite slope is therefore the same as any other vertical column, and can be treated as typical of the entire potential sliding mass.

Figure 2(a) shows the general configuration and forces acting on a typical slice of a $c'-\varphi'$soil of width L, where H and β are the depth and inclination of the potential failure plane, d_w is the depth of the water surface, which in this study is assumed parallel to the ground surface, and γ_{sat}, γ_m and γ' are, respectively, the saturated, moist and buoyant unit weights of the soil, respectively. Figure 2(b) shows the steady flow net and the expression used to compute the pore pressure at any depth below the water surface.

From considerations of limiting equilibrium,

$$\mathrm{FS}=\frac{c'}{((H-d_w)\gamma_{sat}+d_w\gamma_m)\cos\beta\sin\beta}+\frac{((H-d_w)\gamma'+d_w\gamma_m)}{((H-d_w)\gamma_{sat}+d_w\gamma_m)}\frac{\tan\phi'}{\tan\beta} \tag{1}$$

is the general equation for the Factor of Safety of an infinite slope with a water surface running parallel to the ground surface and different soil unit weights above and below the water surface.

If it is conservatively assumed that $\gamma_m \approx \gamma_{sat}$, the equation simplifies to

$$\mathrm{FS}=\frac{c'}{H\gamma_{sat}\cos\beta\sin\beta}+\frac{(H\gamma_{sat}-(H-d_w)\gamma_w)}{H\gamma_{sat}}\frac{\tan\phi'}{\tan\beta} \tag{2}$$

2.1. *Pore pressure parameter* r_u

An alternative way of defining the pore pressures on the potential failure plane (e.g. [23]) is through the pore pressure parameter r_u defined in general as

$$r_u=\frac{u}{\sigma_v} \tag{3}$$

where σ_v is the vertical total stress.

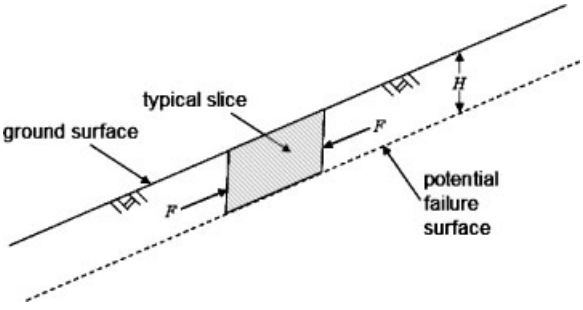

Figure 1. Layout of the infinite slope problem showing a typical slice with equal and opposite side forces.

DOI: 10.1002/nag

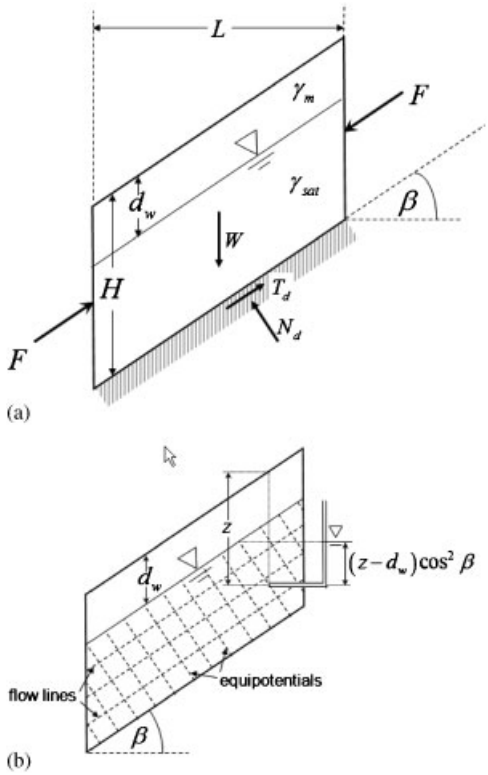

Figure 2. (a) Dimensions and forces acting on a typical slice with a water surface and steady seepage parallel to the ground surface and (b) the steady flow net and the expression used to compute the pore pressure at any depth below the water surface.

For the case shown in Figure 2(b) with steady seepage parallel to the ground surface, it is easily shown that

$$r_{\mathrm{u}} = \frac{(H - d_{\mathrm{w}})\gamma_w \cos^2\beta}{H\gamma_{\mathrm{sat}}} \tag{4}$$

which after substitution into Equation (2) gives

$$\mathrm{FS} = \frac{c'}{\gamma_{\mathrm{sat}} H \cos\beta \sin\beta} + \left(1 - \frac{r_{\mathrm{u}}}{\cos^2\beta}\right)\frac{\tan\phi'}{\tan\beta} \tag{5}$$

It can be noted from Equation (4), that in the case of steady seepage parallel to the ground surface with the water surface at depth d_{w}, r_{u} is also a function of the slope angle β.

3. OBSERVATIONS ON THE INFINITE SLOPE EQUATIONS

3.1. Infinite slope charts

A rearrangement of Equation (5) can be obtained by dividing through by $\tan\phi'$ to give

$$\frac{\mathrm{FS}}{\tan\varphi'} = \frac{c'}{\gamma H \tan\varphi'}\frac{1}{\cos\beta\sin\beta} + \left(1 - \frac{r_{\mathrm{u}}}{\cos^2\beta}\right)\frac{1}{\tan\beta} \tag{6}$$

DOI: 10.1002/nag

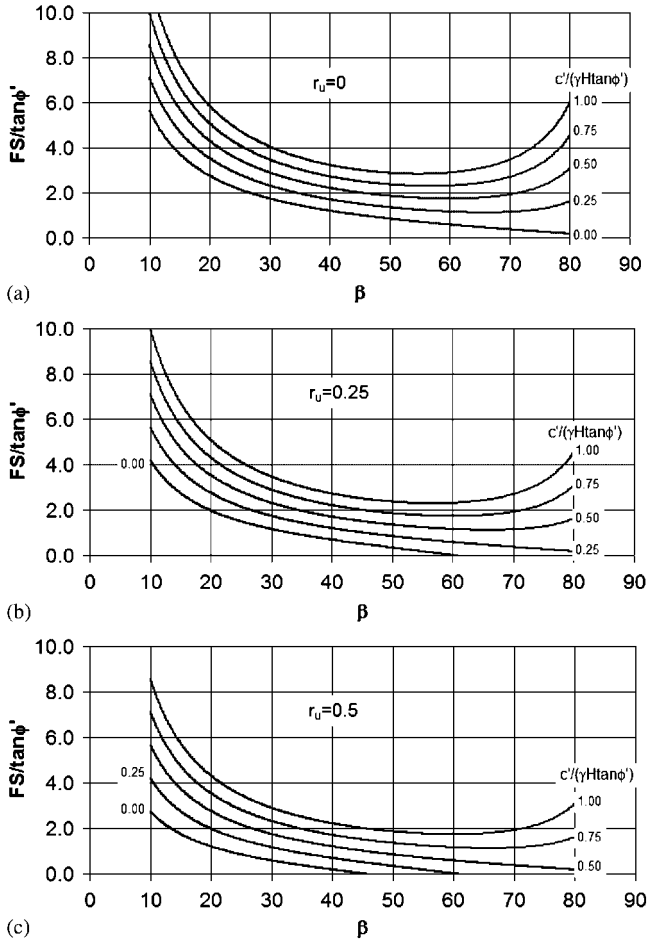

Figure 3. Plots of Equation (7) for (a) $r_u = 0$; (b) $r_u = 0.25$; and (c) $r_u = 0.5$.

where the unit weight $\gamma = \gamma_{sat}$ if the soil is assumed to be saturated ($r_u > 0$), and $\gamma = \gamma_m$ if not ($r_u = 0$). Charts for finite slopes have been developed in this form (e.g. [24]) since it conveniently isolates the slope angle β and highlights the dimensionless group

$$S = c'/(\gamma H \tan \varphi') \tag{7}$$

A graphical representation of this equation has been plotted in Figure 3 for r_u values set, respectively, to 0.0, 0.25 and 0.5.

The figures highlight a curiosity of the infinite slope equations in which a minimum factor of safety is observed at a particular value of the slope angle $\beta = \beta_{min}$. This result may be counter intuitive, since our experience of ordinary slopes is that the factor of safety always falls as a slope gets steeper. An explanation of this effect for infinite slopes comes from the fact that as the slope gets steeper, the length of the potential failure surface available to resist sliding is increasing at a faster rate than the down-slope component of soil weight trying to cause sliding. This phenomenon will be considered again later in the paper.

3.2. The critical slope angle β_{min}

The previous section showed that the infinite slope equations lead to a critical slope angle β_{min} at which the factor of safety reaches a minimum. For slope angles $\beta > \beta_{min}$ the factor of safety starts to rise again. The critical slope angle is easily obtained analytically by finding the minimum of

DOI: 10.1002/nag

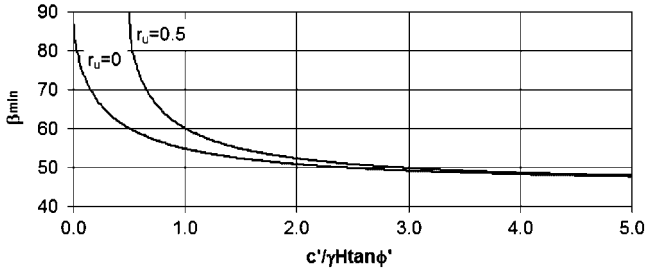

Figure 4. Plot of Equation (8) for $r_u = 0$ and $r_u = 0.5$ indicating the location of the critical slope angle β_{min} for different values of $c'/(\gamma H \tan\phi')$.

the function given in Equation (6). Computer algebra software can facilitate such a calculation to give the critical slope angle as:

$$\beta_{min} = \arccos\left(\sqrt{\frac{S - r_u}{2(S - r_u + 1)}}\right) \quad \text{for } S \geqslant r_u \tag{8}$$

The function shown in Equation (8) is plotted in Figure 4 for the cases when $r_u = 0$ and $r_u = 0.5$ It shows that in all cases $\beta_{min} > 45°$ with $\beta_{min} \to 45°$as $S \to \infty$ (e.g. undrained clay where ϕ' is replaced by $\phi_u = 0$). In addition, a minimum only exists for $S \geqslant r_u$ with $\beta_{min} \to 90°$ as $S \to r_u$.

4. FINITE ELEMENT ANALYSIS OF INFINITE SLOPES[‡]

The starting point for the infinite and long slope program development was an existing program for the analysis of finite slopes using the strength reduction approach (e.g. [25]). This is a technique in which the application of gravity loading is followed by a systematic reduction in soil strength until failure occurs. This is achieved using a *strength reduction factor* SRF which is applied to the frictional and cohesive components of strength in the form

$$\phi'_f = \arctan\left(\frac{\tan\phi'}{\text{SRF}}\right) \quad \text{and} \quad c'_f = \frac{c'}{\text{SRF}} \tag{9}$$

The factored soil properties ϕ'_f and c'_f are the properties actually used during strength reduction, so each trial SRF involves a separate finite element analysis. When slope failure occurs, as indicated by an inability of the algorithm to find an equilibrium stress field that satisfies the Coulomb failure criterion, coupled with significantly increasing nodal displacements, the factor of safety is given by:

$$\text{FS} \approx \text{SRF} \tag{10}$$

The interested reader is referred to other references (e.g. [18]) for more detailed information on the elasto (visco)-plastic and the strength reduction algorithms used in this investigation.

This section will focus on the novel features of the finite element program developed for infinite slope analysis, which lie primarily in the treatment of boundary conditions and gravity loading. The constitutive model is elastic-perfectly plastic and calls for six soil parameters as indicated in Table I. In the current work we have assumed an associated flow rule, so the dilation angle is set equal to the friction angle ($\psi = \phi$) throughout.

A typical mesh for infinite slope analysis consists of a column of 4-node plane strain quadrilateral elements as shown in Figure 5(a). The elements are all congruent parallelograms, which can be assigned different soil properties if required.

[‡]A full source code listing of the infinite slope program described in this paper can be obtained from the first author's web site at `www.mines.edu/~vgriffit/infinite`.

DOI: 10.1002/nag

Table I. Six parameter soil model.

Friction angle	ϕ' or ϕ_u
Cohesion	c'or c_u
Unit weight	γ_{sat} or γ_m
Dilation angle	$\psi = \phi'$
Young's modulus	E' or E
Poisson's ratio	υ' or υ

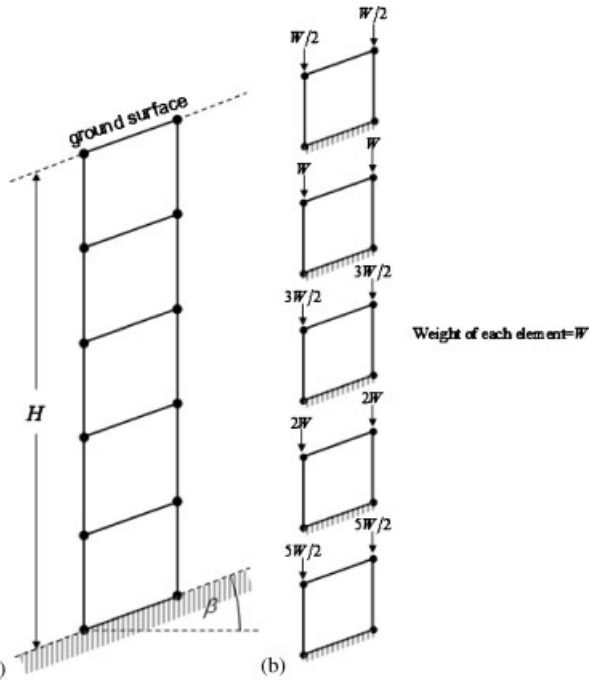

Figure 5. (a) Typical mesh of five identical four-node quadrilateral elements. The program allows the user to decide how many elements to include in the column and (b) the uncoupled analysis treats each element independently with gravity loading applied to the top of each element as shown. Only one element is needed for homogeneous soil profiles.

In order to reproduce the unique side boundary conditions of a soil slice within an infinite slope, an approach has been used whereby the elements are 'uncoupled' from their neighbors as shown in Figure 5(b). Although the element at the bottom of the column is the only one that is truly fixed at its base, this formulation treats all the elements as if they are fixed at their bases, allowing shear stresses and possible shear failure to occur while preserving equivalent boundary conditions on the uphill and downhill sides of the column. The element stiffness matrices are integrated in the usual way (four Gauss-points), however, for purposes of computing stresses, a single stress-point is considered at the centroid of each element. Figure 5(b) also shows how gravity loads are applied to this uncoupled system so as to generate self weight stresses at each stress-point. The loads applied to the top of each element are set equal the total weight of all the elements above and *including* the current element. In this way the stress-points are loaded as if they were at the bottom of each element.

Although each element is uncoupled from its neighbors and develops its own displacements, once a converged solution has been obtained, the global displacements are then accumulated from bottom to top, allowing the deformed mesh or the nodal displacement vectors to be plotted. The ability to predict the factor of safety *and* deformations is s significant advantage of the finite element approach over a simple application of the infinite slope equations which implicitly assume rigid-plastic behavior.

DOI: 10.1002/nag

5. IMPLEMENTATION OF THE INFINITE SLOPE PROGRAM

This section provides some examples of infinite slope analysis in which finite element results are compared with results from the analytical solutions reviewed previously. Homogeneous soils are considered first, but the benefits of the finite element approach are emphasized most effectively in later examples where soil properties are varied with depth. In all cases (effective and total stress analyses) Young's modulus and Poisson's ratio were set to $10^5 \mathrm{kN/m^2}$ and 0.3, respectively, since they have little influence on the computed factor of safety.

5.1. *Total stress analysis*: $\phi_u = 0$, c_u *soil*

In this case the general Equation (5) simplifies to

$$\mathrm{FS} = \frac{c_u}{\gamma_{sat} H \cos\beta \sin\beta} \tag{11}$$

The properties used in this example are $\phi_u = 0$, $c_u = 25\,\mathrm{kN/m^2}$, $\gamma_{sat} = 20\,\mathrm{kN/m^3}$, with a soil depth of $H = 2.5\,\mathrm{m}$ and slope angle $\beta = 30°$. Figure 6 shows typical results from a finite element analysis where the strength reduction factor (SRF) is plotted against the maximum nodal displacement in the mesh. As the SRF is gradually increased, the nodal displacements suddenly increase when $SRF = 1.15$, indicating a factor of safety of $\mathrm{FS} = 1.15$ in close agreement with Equation (11). This result was obtained using a single finite element which is all that is needed for a homogeneous soil layer.

Further comparisons are shown in Figure 7 where the slope angle is varied in the range $10° < \beta < 80°$. The smooth line is from Equation (11) and the plotting points come from the finite element results. As expected for the case when $\phi_u = 0 \quad (S = \infty)$ from equation (8), the minimum factor of safety occurs at $\beta_{min} = 45°$.

5.2. *Effective stress analysis*: $c' - \phi'$ *soil with a free-surface at mid-depth* ($d_w = 0.5\ H$)

Assuming saturated soil above and below the water surface, the system is governed by Equation (2):

$$\mathrm{FS} = \frac{c'}{H\gamma_{sat} \cos\beta \sin\beta} + \frac{(H\gamma_{sat} - (H - d_w)\gamma_w)}{H\gamma_{sat}} \frac{\tan\phi'}{\tan\beta} \tag{12}$$

The properties used in this example are $\phi' = 30°$, $c' = 10\,\mathrm{kN/m^2}$, $\gamma_{sat} = 18\,\mathrm{kN/m^3}$, $d_w = 2.5\,\mathrm{m}$ and $H = 5\,\mathrm{m}$ with a slope angle $\beta = 25°$. In the finite element analysis, the pore pressure at the base of each element is computed using the formula shown in Figure 2(b) with results shown in Figure 8. Both finite elements and the analytical solution from Equation (12) give $\mathrm{FS} = 1.19$.

Further comparisons are shown in Figure 9 where the slope angle is varied in the range $10° < \beta < 80°$. The smooth line comes from Equation (12) and the plotting points come from the finite

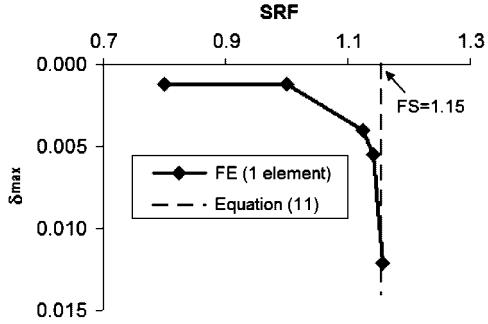

Figure 6. Strength reduction factor vs maximum nodal displacement for an infinite slope with of undrained clay with $\phi_u = 0$, $c_u = 25\,\mathrm{kN/m^2}$, $\gamma_{sat} = 20\,\mathrm{kN/m^3}$, $H = 2.5\,\mathrm{m}$ and $\beta = 30°$.

DOI: 10.1002/nag

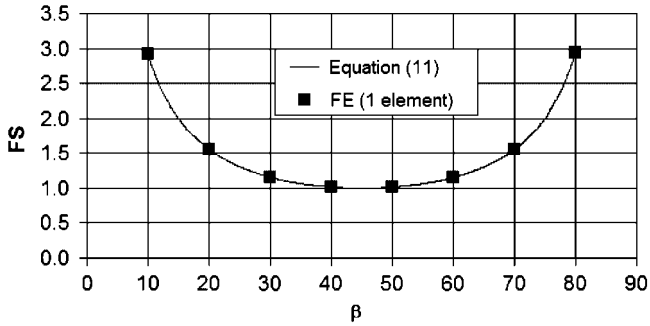

Figure 7. Comparison of finite element and analytical solutions for an infinite slope of undrained clay with $\phi_u = 0$, $c_u = 25\text{kN/m}^2$, $\gamma_{sat} = 20\text{kN/m}^3$ and $H = 2.5\text{m}$ over a range of the slope angles β.

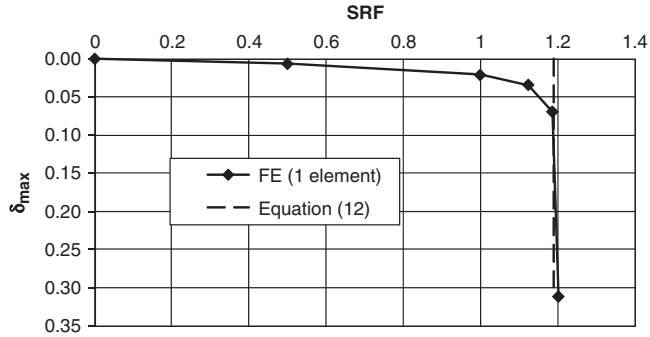

Figure 8. Strength Reduction Factor vs maximum nodal displacement for an infinite slope with $\phi' = 30°$, $c' = 10\text{kN/m}^2$, $\gamma_{sat} = 18\text{kN/m}^3$, $d_w = 2.5\text{m}$, $H = 5\text{m}$ and $\beta = 25°$.

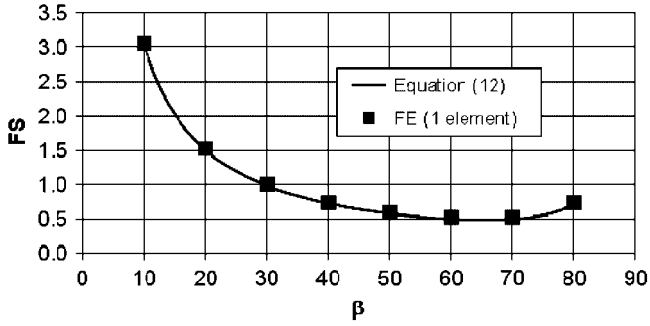

Figure 9. Comparison of finite element and analytical solutions from Equation (13) for an infinite slope with $\phi' = 30°$, $c' = 10\text{kN/m}^2$, $\gamma_m = 18\text{kN/m}^3$, $d_w = 2.5\text{m}$ and $H = 5\text{m}$ over a range of the slope angles β.

element runs for values of β at 10° intervals. By differentiation of Equation (12) and equating the result to zero, the minimum factor of safety can be shown to occur when the slope angle is close to $\beta_{min} = 65°$. It may be noted that for the case when the water depth d_w is held constant, the pore pressure parameter r_u from Equation (4) becomes a function of the slope angle β.

5.3. *Effective stress analysis*: c'-ϕ' *soil with pore pressures* ($r_u = 0.5$)

Assuming saturated soil above and below the water surface, the system is governed by Equation (5).

DOI: 10.1002/nag

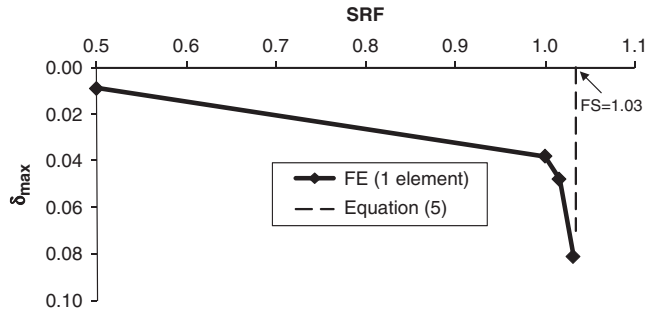

Figure 10. Strength reduction factor vs maximum nodal displacement for an infinite slope with $\phi' = 30°$, $c' = 20\,\text{kN/m}^2$, $\gamma_{\text{sat}} = 19\,\text{kN/m}^3$, $r_u = 0.5$, $H = 5\,\text{m}$ and $\beta = 25°$.

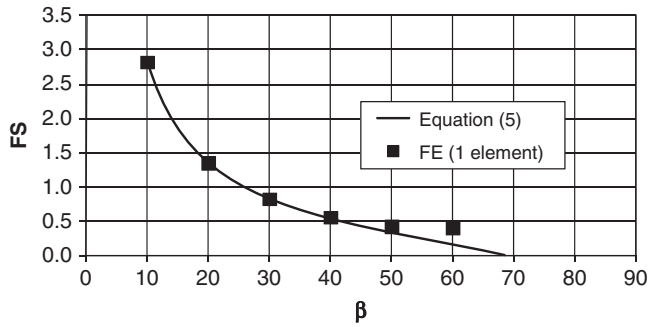

Figure 11. Comparison of finite element and analytical solutions from Equation (14) for an infinite slope with $\phi' = 30°$, $c' = 20\,\text{kN/m}^2$, $\gamma_{\text{sat}} = 19\,\text{kN/m}^3$, $r_u = 0.5$ and $H = 5\text{m}$ over a range of the slope angles β.

The properties used in this example are $\phi' = 30°$, $c' = 20\,\text{kN/m}^2$, $\gamma_{\text{sat}} = 19\,\text{kN/m}^3$, $r_u = 0.5$, $H = 5\text{m}(S = 0.365)$ with a slope angle of $\beta = 25°$. Figure 10 shows typical results from a finite element analysis compared with the analytical solution from equation (5) which gives FS = 1.03.

Further comparisons are shown in Figure 11 where the slope angle is varied in the range $10° < \beta < 80°$. The smooth line comes from Equation (5) and the plotting points come from the finite element runs for values of β at 10° intervals. Good agreement between the solutions is obtained until the steepness of the slope exceeds about 50° when the analytical values of FS from Equation (5) become very small. The finite element solutions perform poorly in this range because the factored shear strength values from equations (9) are becoming very high. For example, when $\beta = 60°$ Equation (5) gives FS = 0.153 which would require a factored friction angle of $\phi'_f = \arctan(\tan 30/0.153) = 75.2°$! It may also be noted in this example that there is no β_{min} solution because $S < r_u$.

5.4. *Effective stress analysis*: c'-ϕ' *soil with parabolically varying* c' *with depth* ($r_u = 0$)

Here we introduce a more complex strength distribution by assuming that c'increases parabolically with depth according to

$$c' = p + qz^2 \tag{13}$$

where $p(>0)$ is the cohesion at the ground surface ($z = 0$), and $q(>0)$, is the constant coefficient of the z^2 term.

Although this may not be a very realistic soil profile, it introduces for the first time in this paper, the possibility of failure occurring at locations above the base of the soil column.

DOI: 10.1002/nag

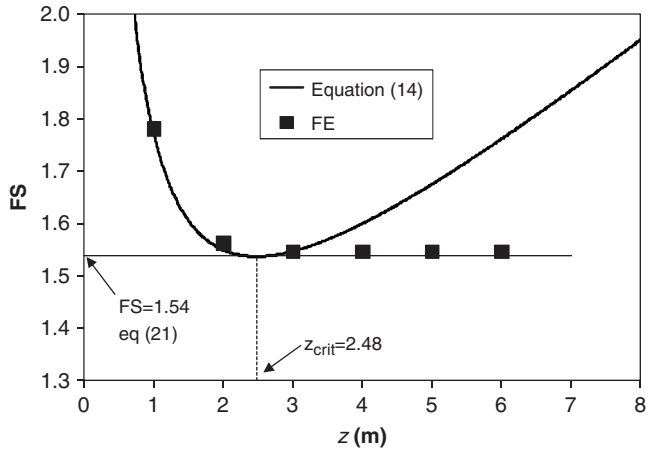

Figure 12. Variation of FS with z for a soil with $\phi' = 25°$, $c' = 4.6 + 0.75z^2\,\mathrm{kN/m^2}$, $\gamma_m = 18\,\mathrm{kN/m^3}$ and $\beta = 25°$. The plot shows that FS initially falls as z increases but reaches a minimum when $z_{crit} = 2.48\,\mathrm{m}$. For $z > z_{crit}$ FS remains constant and equal to 1.54.

To find the depth of the critical failure plane, substitute Equation (13) into Equation (5) and replace H by z to give

$$\mathrm{FS} = \frac{p + qz^2}{\gamma_m z \cos\beta \sin\beta} + \frac{\tan\varphi'}{\tan\beta} \tag{14}$$

and solve $(\partial(\mathrm{FS})/\partial z) = 0$ for z_{crit} to find the critical depth that gives the minimum value of FS. Hence

$$z_{crit} = \sqrt{\frac{p}{q}} \tag{15}$$

and

$$\mathrm{FS} = \frac{2\sqrt{pq}}{\gamma_m \cos\beta \sin\beta} + \frac{\tan\varphi'}{\tan\beta} \tag{16}$$

This is in agreement with the observation (e.g. [26]) that the critical failure plane for constant ϕ'develops where c'/z reaches a minimum.

Consider the case where $\phi' = 25°$, $c' = 4.6 + 0.75z^2\,\mathrm{kN/m^2}$ ($p = 4.6$, $q = 0.75$), $\gamma_m = 18\,\mathrm{kN/m^3}$ and $\beta = 25°$. For these properties, Equations (15) and (16) give $z_{crit} = 2.48\,\mathrm{m}$ and $\mathrm{FS} = 1.54$, respectively. A column of 10 elements per meter of depth was used to model the parabolic variation of $c'$with z. The variation of FS with z from Equation (14) is shown in Figure 12 together with the finite element solutions.

This case demonstrates that for soil depths $z < z_{crit}$ the critical failure plane occurs at depth z and the factor of safety is given by Equation (14), while for soil depths $z \geqslant z_{crit}$ the factor of safety remains fixed at the value given by Equation (16).

An initial and deformed mesh at failure is shown in Figure 13. Although the mesh remains continuous, the location of the failure plane at the critical depth of $z_{crit} = \sqrt{\frac{4.6}{0.75}} = 2.48\,\mathrm{m}$ from Equation (15) is clearly indicated. In this case, multiple elements in the finite element discretization of the soil column are needed to 'capture' the critical mechanism.

6. FINITE ELEMENT ANALYSIS OF LONG SLOPES

In this section some conventional finite element slope stability analyses have been performed on long slopes with more realistic boundary uphill and downhill conditions, to assess the range of

DOI: 10.1002/nag

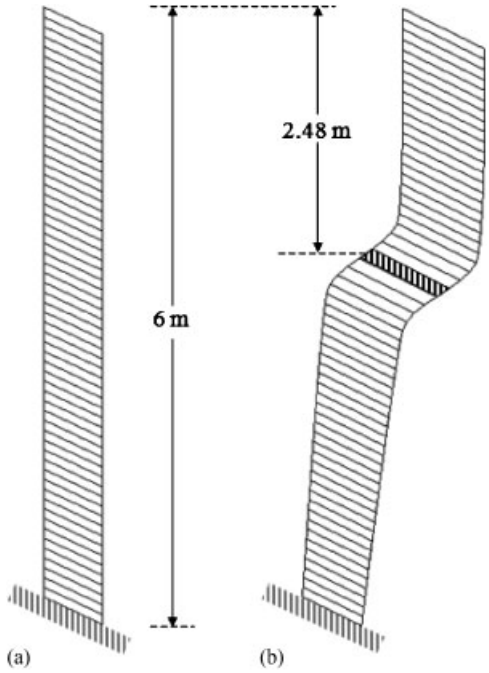

Figure 13. (a) Initial mesh of 60, 4-node elements and with $H=6\,\mathrm{m}$ and $\beta=25°$ for a soil with $\phi'=25°$, $c'=4.6+0.75z^2\,\mathrm{kN/m^2}$ and $\gamma_m=18\,\mathrm{kN/m^3}$ and (b) deformed mesh at failure indicating the formation of a failure plane at an intermediate depth of $z_{crit}=2.48\,\mathrm{m}$.

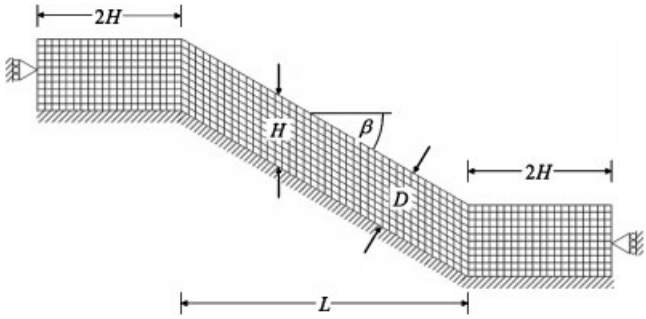

Figure 14. Typical mesh of 8-node quadrilateral element for 'long slope' analysis.

validity and conservatism of the infinite slope assumptions. Questions addressed in this section are as follows: (i) How long must a slope be for it to be considered 'infinite'? (ii) Is there a critical slope angle at which the factor of safety reaches a minimum as indicated by the infinite slope equations (e.g. Figure 3)?

It has been noted previously (e.g. [26]) that the infinite slope assumptions can be expected to lead to conservative estimates of the factor of safety. This is primarily due to support provided at the ends of a finite slope that is not accounted for in the infinite slope model.

A typical finite element mesh of 8-noded quadrilateral elements is shown in Figure 14 consisting of horizontal sections to the left and right, and a long sloping central section. The base of the mesh is fully fixed and the extreme vertical boundaries to the left and right allow vertical movement only. Other boundary conditions, for example, allowing the end sections to be sloping, have been considered by [27]) but are not reported here.

The geometry was set up so that the dimensions and mesh refinement of the various sections could easily be modified through the data. A very large number of parametric variations are possible

DOI: 10.1002/nag

in such a study, but in this section, and for consistency with the infinite slope results presented previously, it was decided that the vertical depth of soil (H) would be held constant while the slope angle (β) and length (L) were varied. In the analyses that follow, two of the examples considered in Section 5 are revisited. In each case parametric studies were performed relating to the dimensionless 'length ratio' which was varied in the range $2 \leqslant L/H \leqslant 32$ and the slope angle (β), which was varied in the range $10° \leqslant \beta \leqslant 80°$. In all cases the mesh refinement was consistent and similar to that shown in Figure 14, where the soil depth was modeled using a column of 10 elements.

6.1. *Total stress analysis*: $\phi_u = 0$, c_u *soil*

This example is similar to the infinite slope case considered previously in Section 5.1. The parameters $H = 2.5\,\text{m}$, $c_u = 25\,\text{kN/m}^2$, $\beta = 30°$ and $\gamma_{sat} = 20\,\text{kN/m}^3$ were held constant while L/H was gradually increased. As shown in Figure 15, the computed factor of safety converged on the infinite slope solution of FS = 1.15 from Equation (11) for L/H greater than about 16. It may be noted that the infinite slope solution is always conservative. For example, with $L/H = 2$ the computed factor of safety was FS = 2.86, more than double the infinite slope value.

Typical deformed meshes at failure in Figure 16 show that for shorter slopes, a significant proportion of the failure mechanism path involves cutting through soil at the top and the bottom of the slope, leading to higher factors of safety. For longer slopes, the majority of the mechanism is parallel to the ground surface and runs along the base of the layer, leading to factors of safety in closer agreement with the infinite slope result.

The influence of the slope angle on the factor of safety for two different length ratios was considered next with results shown in Figure 17. The infinite slope solution from Equation (11)

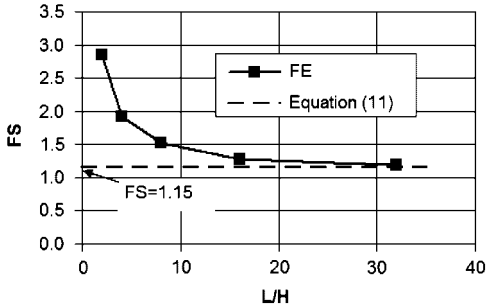

Figure 15. Influence of length ratio L/H on the computed factor of safety FS for slope with $H = 2.5\,\text{m}$, $\beta = 30°$, $c_u = 25\,\text{kN/m}^2$ and $\gamma_{sat} = 20\,\text{kN/m}^3$.

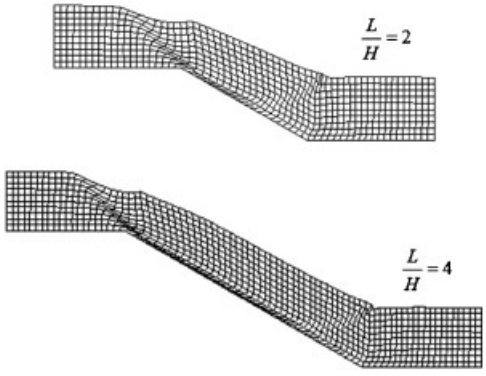

Figure 16. Deformed meshes at failure for the cases of $L/H = 2$ and $L/H = 4$ showing how the infinite slope mechanism becomes more dominant for the longer slope.

DOI: 10.1002/nag

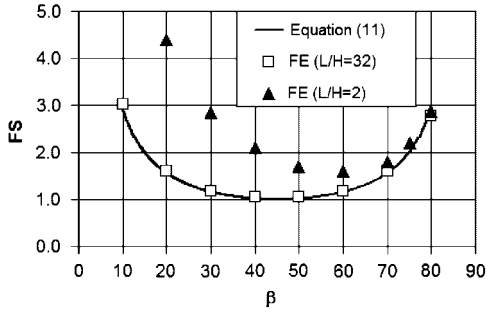

Figure 17. Influence of slope angle β on the computed factor of safety FS for an undrained clay slope with $H=2.5\,\mathrm{m}$, $c_u=25\,\mathrm{kN/m^2}$ and $\gamma_{sat}=20\,\mathrm{kN/m^3}$ for two different length ratios.

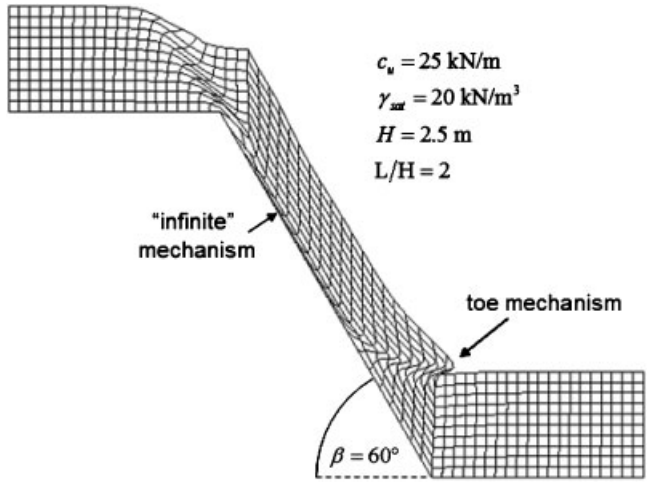

Figure 18. Deformed mesh at failure corresponding to a slope with $L/H=2$ and $\beta=60°$ indicating a toe mechanism with FS = 1.58.

is also shown in this figure. The long slope with $L/H=32$ agreed with the infinite slope solution over the full range of slope angles considered. The 'short' slope with $L/H=2$ gave significantly higher factors of safety than the long slope at flatter slope angles. Less predictably, the factor of safety in the short slope analysis also exhibited a minimum at $\beta\approx60°$ of about FS = 1.58 before rising again at higher slope angles. All three solutions essentially converged on the same factor of safety of FS = 2.88 for the steepest slope considered ($\beta=80°$).

For most short slopes, the failure mechanism is attracted to the toe of the slope as shown in Figure 18, which gives the deformed mesh at failure for $L/H=2$ and $\beta=60°$, corresponding to the minimum FS = 1.58. For very steep slopes however, the toe mechanism is no longer dominant and the critical mechanism changes to a localized failure at the top of the slope as shown by the displacement vectors in Figure 19 for $\beta=75°$, which gave FS = 2.20. This type of mechanism is more reminiscent of a 'vertical cut' failure and is not affected by the value of L/H.

6.2. *Effective stress analysis*: c'-ϕ' *soil with pore pressures* ($r_u=0.5$)

This example is similar to the infinite slope case considered in Section 5.3, and the results are qualitatively similar to those obtained in Section 6.1 for an undrained clay slope.

Parameters given by $H=5.0\,\mathrm{m}$, $\phi'=30°\mathrm{c}'=20\,\mathrm{kN/m^2}$, $r_u=0.5$, $\gamma_{sat}=19\,\mathrm{kN/m^3}$ and $\beta=25°$ were held constant while L/H was gradually increased. As shown in Figure 20, as the length ratio

DOI: 10.1002/nag

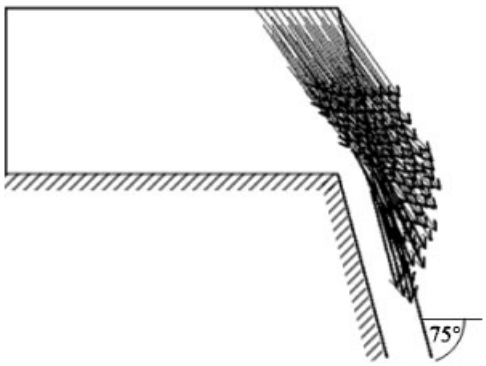

Figure 19. Detail of the nodal displacement vectors at failure at the top of a very steep slope with $\beta \approx 75°$ giving FS = 2.20.

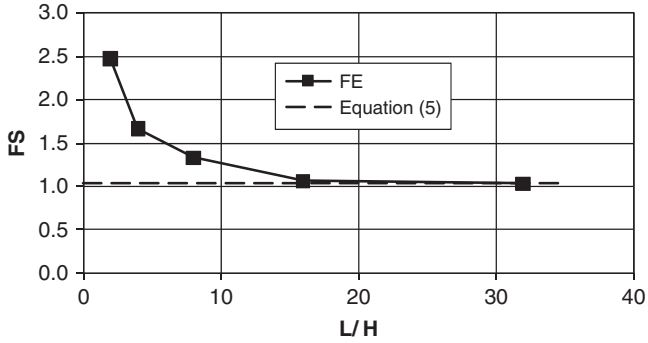

Figure 20. Influence of length ratio L/H on the computed factor of safety FS for slope with $\phi' = 30°$, $c' = 20\text{kN/m}^2$, $\gamma_{sat} = 19\text{kN/m}^3$, $r_u = 0.5$, $H = 5\text{m}$ and $\beta = 25°$.

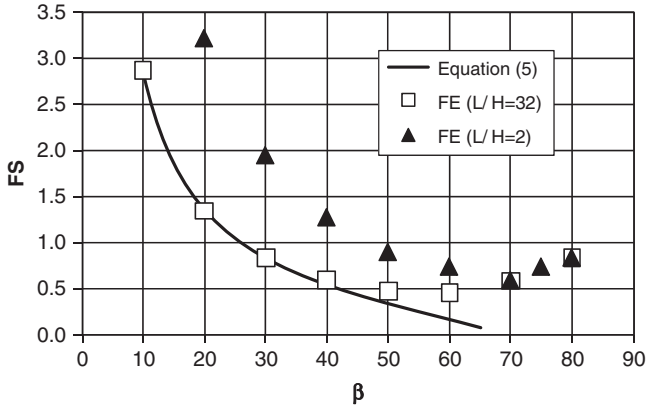

Figure 21. Influence of slope angle β on the computed factor of safety FS for long slopes with $\phi' = 30°, c' = 20\text{kN/m}^2, \gamma_{sat} = 19\text{kN/m}^3, r_u = 0.5$ and $H = 5\text{m}$ over a range of the slope angles β.

increased, the computed factor of safety converged on the infinite slope solution of FS = 1.03 from Equation (5). As before, good agreement with the infinite slope result was achieved for $L/H > 16$.

The influence of the slope angle on the factor of safety for two different length ratios was considered next with results shown in Figure 21. The infinite slope solution from Equation (5) is also shown in this figure. The long slope with $L/H = 32$ agreed closely with the infinite slope solution for relatively flat slopes. For $\beta > 40°$; however, while the factor of safety predicted

DOI: 10.1002/nag

by the infinite slope equation continued to fall towards zero, the long slope solution reached a minimum factor of safety and started to increase. As expected, the shorter slope with $L/H=2$ gave significantly higher factors of safety at flatter slope angles but as the slope angle increased, it too reached a minimum value at around $\beta=70^\circ$ before rising to converge with the longer slope solution at a factor of safety of about FS$=0.83$. Clearly from a practical point of view, FS<1 implies an unstable slope that could never exist, but it is the qualitative behavior of these results, and particularly the minimum in the FS response that is of interest.

7. CONCLUDING REMARKS

The paper has revisited the infinite slope equations and compared analytical results with finite element solutions for infinite and long slopes. Examples including groundwater modeled through a free-surface or an r_u parameter were also considered. For numerical modeling of the infinite slope problem, a novel finite element approach was described for modeling the 'infinite' boundary conditions on both sides of a typical soil slice. The benefits and generality of the finite element approach were particularly emphasized in examples where the soil strength profile varied with depth and where the location of the critical failure surface was not known *a priori*. The finite element solutions also gave a clear indication of the location of the critical failure plane.

The second half of the paper assessed the conservatism of the infinite slope equations by performing conventional finite element slope stability analyses on long finite slopes with more realistic uphill and downhill boundary conditions. The analyses confirmed that the infinite slope equations are always conservative, however the factors of safety predicted by finite element analysis of long slopes approached the infinite slope solutions for length ratios in the order of $L/H>16$.

Additional studies were performed to assess the role of the slope angle β on the factor of safety of long and infinite slopes. These studies confirmed the existence of a minimum factor of safety corresponding to a critical slope angle $\beta_{\min}$. While this phenomenon is predicted by the infinite slope equations, the minimum was also observed for shorter slopes, suggesting the counter-intuitive observation that very steep long slopes may actually be 'safer' than flatter slopes. Insight into this phenomenon was provided by the finite element solutions which showed that the mechanism tended to outcrop at the toe of the slope for flatter slopes, but changed to a 'vertical cut'-type mechanism for very steep slopes where the length ratio L/H became irrelevant.

While it inconceivable that engineers would ever rely on the 'steeper is safer' effect in constructed slopes, the phenomenon is certainly of theoretical interest for long slopes, and may give insight into the optimal angle at which landslides and other natural slope failures are most likely to occur.

NOMENCLATURE

The following symbols are used in this paper:

c'	soil cohesion
c'_f	factored soil cohesion
c_u	undrained shear strength
d_w	depth of the water surface
E'	Young's modulus
FS	factor of safety
FS_{min}	minimum factor of safety
H	depth of the soil layer
H_{crit}	critical depth of the failure plane
L	width of slice
N_d	normal force component

DOI: 10.1002/nag

p	factor used to describe variation of cohesion with depth
q	cohesion at ground surface
r_u	pore pressure parameter
S	dimensionless group, $c'/(\gamma H \tan\phi')$
SRF	strength reduction factor
T_d	shear force component
u	pore pressure
z	depth coordinate
W	weight of slice
β	slope inclination
$\beta_{\min}$	slope angle leading to FS_{min}
γ'	buoyant unit weight
γ_m	moist (or dry) unit weight
γ_{sat}	saturated unit weight
γ_w	unit weight of water
$\delta_{\max}$	maximum nodal displacement
θ	inclination of seepage to the ground surface
σ	normal total stress
σ'	normal effective stress
σ_v	vertical total stress
τ_d	developed shear stress
τ_f	shear strength
υ	Poisson's ratio
ϕ'	soil friction angle
ϕ'_f	factored friction angle
ϕ_u	undrained friction angle (=0)
ψ	dilation angle

ACKNOWLEDGEMENTS

The authors wish to acknowledge the support of NSF grant CMS-0408150 on 'Advanced probabilistic analysis of stability problems in geotechnical engineering'.

REFERENCES

1. Turner AK, Schuster RL (eds). *Proceedings of the 1st North American Landslide Conference*, *Landslides and Society*, *AEG Special Publication No. 22*. Association of Environmental and Engineering Geologists: Denver, CO, 2007; 261–276.
2. Teunissen JAM, Spierenburg SEJ. Stability of infinite slopes. *Géotechnique* 1995; **45**(2):321–323.
3. Christian JT, Whitman R. One-dimensional model for progressive failure. *Proceedings of the 7th ICSMFE*, Mexico, 1969; 541–545.
4. Mello UT, Pratson LF. Regional slope stability and slope-failure mechanics from the two-dimensional state of stress in infinite slope. *Marine Geology* 1999; **154**:339–356.
5. Urciuoli G. Strain preceding failure in infinite slope. *International Journal of Geomechanics* 2002; **2**(1):93–112.
6. Runesson LA, Wiberg LA. Stability analysis of natural slopes in clay by use of the finite element method. *Report 84*, Department of Structural Mechanics, Chalmers University of Technology, Göteborg, 1984.
7. Wiberg NE, Koponen M, Runesson K. Finite element analysis of progressive failure in long slopes. *International Journal for Numerical and Analytical Methods in Geomechanics* 1990; **14**:599–612.
8. Iverson RM. Groundwater flow fields in infinite slopes. *Géotechnique* 1990; **40**(1):139–143.
9. Wallach R, Zaslavsky D. Lateral flow in a layered Profile of a infinite uniform slope. *Water Resources Research* 1991; **27**(8):1809–1818.
10. Bromhead EN, Martin PL. Three dimensional equilibrium analysis of the Taren landslide. *Advances in Geotechnical Engineering*: *The Skempton Conference*, vol. 2. Thomas Telford ICE: Reston, 2004.
11. Cho SE, Lee SR. Evaluation of surficial stability for homogeneous slopes considering rainfall characteristics. *Journal of Geotechnical and Geoenvironmental Engineering* (ASCE) 2002; **128**:756–763.

DOI: 10.1002/nag

12. Collins BD, Znidarcic D. Stability analyses of Rainfall induced landslides. *Journal of Geotechnical and Geoenvironmental Engineering* (ASCE) 2004; **130**:362–372.
13. Tsai TL, Yang JC. Modeling of rainfall-triggered shallow landslide. *Environmental Geology* 2006; **50**(4):525–534.
14. Yang J. On seismic landslide hazard assessment. *Géotechnique* 2007; **57**(8):707–713.
15. Zienkiewicz OC, Humpheson C, Lewis RW. Associated and non-associated visco-plasticity and plasticity in soil mechanics. *Géotechnique* 1975; **25**(4):671–689.
16. Griffiths DV. Finite element analysis of walls, footings and slopes. *Computer Applications to Geotechnical Problems in Highway Engineering Cambridge Symposium*, 1980. PM Geotechnical Analysts Ltd: Cambridge, 1981; 122–146.
17. Matsui T, San KC. Finite element slope stability analysis by shear strength reduction technique. *Soils and Foundations* 1992; **32**(1):59–70.
18. Griffiths DV, Lane PA. Slope stability analysis by finite elements. *Géotechnique* 1999; **49**(3):387–403.
19. Bromhead EN. *The Stability of Slopes* (2nd edn). Blackie Academic and Professional: London, New York, 1992; 135–137.
20. Taylor DW. *Fundamentals of Soil Mechanics*. Wiley: Hoboken, NJ, 1948.
21. Lambe TW, Whitman RV. *Soil Mechanics*. Wiley: New York, 1969; 553.
22. Duncan JM. Slope stability analysis. *Landslide Investigation and Mitigation*, Chapter 13. National Research Council. National Academy Press: Washington, DC, 1996. Special Report 247, TRB.
23. Bishop AW, Morgenstern N. Stability coefficients for earth slopes. *Géotechnique* 1960; **10**(4):129–150.
24. Michalowski RL. Stability Chart for uniform slope. *Journal of Geotechnical and Geoenvironmental Engineering* 2002; **128**(4):351–355.
25. Smith IM, Griffiths DV. *Programming the Finite Element Method* (4th edn). Wiley: West Sussex, England, 2004.
26. Duncan JM, Wright SG. *Soil Strength and Slope Stability*. Wiley: Hoboken, NJ, 2005.
27. Griffiths DV, Denavit MD. Probabilistic analysis and finite element modeling of infinite slopes. In *Proceedings of the 1st North American Landslide Conference. Landslides and Society*, Turner AK, Schuster RL (eds). Association of Environmental and Engineering Geologists: Denver, CO, 2007; 261–276. AEG Special Publication No. 22.

DOI: 10.1002/nag